HHS Public Access

Author manuscript

Brain Res. Author manuscript; available in PMC 2018 February 27.

Published in final edited form as:

Brain Res. 2014 October 17; 1585: 51–62. doi:10.1016/j.brainres.2014.06.021.

Physical Activity Correlates with Glutamate Receptor Gene Expression in Spinally-Projecting RVLM Neurons: A Laser Capture Microdissection Study

Madhan Subramanian[1], **Avril G. Holt**[2], and **Patrick J. Mueller**[1]

[1]Department of Physiology, Wayne State University School of Medicine, Detroit, MI 48201, USA

[2]Department of Anatomy and Cell Biology, Wayne State University School of Medicine, Detroit, MI 48201, USA

Abstract

Physical inactivity is an important risk factor in the development of cardiovascular disease. The rostral ventrolateral portion of the medulla (RVLM) is composed of heterogeneous populations of neurons that are involved in the regulation of the cardiovascular system. Because of functional heterogeneity, studying the changes in the gene expression of this specific population of neurons within the RVLM is challenging. In the present study, a fluorescent retrograde tracer was injected into the spinal cord to specifically label bulbospinal RVLM neurons in sedentary and active rats. Laser capture microdissection (LCM) was then employed to collect the fluorescently labeled neurons from sections encompassing the rostrocaudal extent of the RVLM. RNA extracted from the neurons was used in qRT-PCR analysis. Changes in gene expression levels of glutamate and GABA receptor subunits were compared between sedentary and physically active rats. GLUR3 subunit showed a significant negative correlation between total running distance and its relative gene expression in active rats. There were no significant difference in the gene expression of NMDA (NR1, NR2A, NR2B, NR2C and NR2D), AMPA (GLUR1, GLUR2 and GLUR3) and $GABA_A$ ($GABA_{A1}$ and $GABA_{A2}$) receptor subunits. Overall, the present study demonstrates the feasibility of utilizing LCM to investigate the gene expression changes in a specific population of neurons in the RVLM. Correlation studies suggest that physical activity could contribute to neuroplasticity in the RVLM.

1. Introduction

Cardiovascular diseases (CVD) are the leading cause of death in the United States. Physical inactivity has been well established as an independent risk factor in the development of CVD. Evidence suggests that central nervous system mechanisms involving overactivity of the sympathetic nervous system contributes to conditions such as hypertension and heart failure (Fisher, Young, and Fadel, 2009;Malpas, 2010;Zucker, Wang, Brandle, Schultz, and Patel, 1995). Recently our group has suggested that physical activity-dependent neuroplastic changes occur at the level of the brainstem and mediate sympathetic overactivity (Martins-

Send correspondence to: Patrick J. Mueller, Ph.D., Department of Physiology, Wayne State University School of Medicine, 540 E. Canfield, Detroit MI 48201, Phone: 313-577-1559, FAX: 313-577-5494, pmueller@med.wayne.edu.

Pinge, Becker, Garcia, Zoccal, Neto, Basso, de Souza, and Lopes, 2005;Mueller, 2010). However the underlying cellular and molecular mechanisms contributing to the alterations in sympathetic outflow remain unclear.

The rostral ventrolateral medulla (RVLM) is an important cardiovascular region of the brainstem involved in tonic and reflex control of blood pressure and sympathetic nerve activity (SNA) (Dampney, 2009;Guyenet, 2006). Presympathetic sympathoexcitatory neurons from the RVLM project to the intermediolateral cell column (IML) located between the first thoracic (T1) and the second lumbar (L2) segments of the spinal cord (Amendt, Czachurski, Dembowsky, and Seller, 1979;Lipski, Kanjhan, Kruszewska, and Smith, 1995). In these regions of the spinal cord, RVLM neurons innervate sympathetic preganglionic neurons in the IML and are involved in cardiovascular regulation (Dampney, 1994;Guyenet and Stornetta, 2004).

The neurotransmitter glutamate is important for the regulation of neuronal activity in the RVLM especially under sympathoexcitatory conditions (Pilowsky, Abbott, Burke, Farnham, Hildreth, Kumar, Li, Lonergan, McMullan, Spirovski, and Goodchild, 2008;Stornetta, Sevigny, Schreihofer, Rosin, and Guyenet, 2002;Sved, 2004). Both the N-methyl-D-aspartate (NMDA) and alpha-amino-3-hydroxy-5-methyl-4-isoxazolepropionic acid (AMPA) subtypes of the glutamate receptor in the RVLM are known to play a major role in the control of cardiovascular activity(Edwards, Loxley, Powers-Martin, Lipski, McKitrick, Arnolda, and Phillips, 2004;Hermes, Mitchell, Silverman, Lynch, McKee, Bailey, Andresen, and Aicher, 2008;Kiely and Gordon, 1993;Miyawaki, Minson, Arnolda, Llewellyn-Smith, Chalmers, and Pilowsky, 1996;Wang, Wang, Gao, and Wang, 2007). Furthermore, NMDA and AMPA receptor neuroplasticity has been observed in several brain regions following sedentary conditions and in disease models such as heart failure (Farmer, Zhao, Van Praag, Wodtke, Gage, and Christie, 2004;Kleiber, Zheng, Schultz, Peuler, and Patel, 2008;Li, Cornish, and Patel, 2003;Malinow and Malenka, 2002;Wang, Gao, Wang, Zucker, and Wang, 2009). Similarly, recent functional studies from our laboratory and others using direct glutamatergic activation of the RVLM have demonstrated enhanced cardiovascular responses in sedentary versus physically active rats (Martins-Pinge, Becker, Garcia, Zoccal, Neto, Basso, de Souza, and Lopes, 2005;Mischel and Mueller, 2011;Mueller and Mischel, 2012). Therefore identifying mechanisms by which glutamatergic neurotransmission is altered by sedentary versus physically active conditions is critical to our understanding of RVLM control of cardiovascular function.

In addition to excitatory neurotransmission, GABA (γ-amino butyric acid) is the major inhibitory neurotransmitter in the RVLM (Dampney, Blessing, and Tan, 1988;Miyawaki, Goodchild, and Pilowsky, 2002). GABAergic inhibition in the RVLM is mediated largely by ionotropic $GABA_A$ and to a lesser extent metabotropic $GABA_B$ receptors (Foley, Stanton, Price, Cunningham, Hasser, and Heesch, 2003;Li and Pan, 2005;Nakamura, Kawabe, and Sapru, 2008). Alterations in the expression of GABAergic receptors of the RVLM could account for changes in SNA under variety of conditions, including physical inactivity (Moffitt, Heesch, and Hasser, 2002;Mueller, 2007;Mueller and Mischel, 2012) and various forms of hypertension (Huber and Schreihofer, 2011;Smith and Barron, 1990).

The RVLM is composed of heterogeneous groups of neurons that serve a wide variety of functions based upon their projections throughout the central nervous system including the spinal cord. In the RVLM, neurons projecting to the spinal cord are essential for cardiovascular control (Guyenet, 2006;Schreihofer and Sved, 2011). However studying alterations in neurotransmitter-related mechanisms within specific neuronal populations (e.g. bulbospinal RVLM neurons) using more traditional techniques such as tissue punches is challenging. Some of these limitations prompted researchers in the late '90s to develop a new technique that employed laser-based microscopy, laser capture microdissection (LCM), to dissect specific cells from complex tissue (Emmert-Buck, Bonner, Smith, Chuaqui, Zhuang, Goldstein, Weiss, and Liotta, 1996). Combining LCM with tract tracing, our goal was to correlate glutamate and GABA receptor gene expression in spinally projecting RVLM (bulbospinal) neurons with level of physical activity using sedentary and active rats.

2. Results

Spinally-projecting RVLM neurons were retrogradely labeled following an injection of Fluorogold into the IML cell column of the spinal cord (Figure 1). The brainstem was cryosectioned and stained using cresyl violet allowing the location of the RVLM to be identified using the large motor neurons of the facial nucleus as a landmark (Figure 2). The boundaries of the RVLM are defined with respect to the caudal pole of the facial nucleus, extending 500 μm caudally and 150 μm rostrally (Figure 1). Only Fluorogold-positive neurons localized within the RVLM with clearly identified nuclei were considered acceptable and were removed using LCM (Figure 3). An average of approximately 700 Fluorogold-positive neurons were collected from both sedentary (709 ± 95 cell profiles) and active (689 ± 88 cell profiles) rats ($p>0.05$) (Figure 4A). The average number of cells captured from the active rats on the right and left side are 360 ± 50 and 329 ± 38 respectively. Similarly, the average number of cells captured from the sedentary rats on the right and left side are 350 ± 29 and 359 ± 66 respectively. Fluorescently labeled cells were captured throughout the classically defined portion of the cardiovascular region of the RVLM (500 μm caudal and 150-μm rostral to the caudal pole of the facial nucleus) (Llewellyn-Smith and Mueller, 2013;Schreihofer and Sved, 2011). However, the majority of the cells collected were from the caudal 500 μm of the RVLM as shown by the rostro-caudal distribution of Fluorogold-positive neurons in sedentary and active (Figure 4B). Interestingly, the average number of Fluorogold-positive neurons collected per slide did not appear different between the sedentary and active rats regardless of location along the rostro-caudal axis of the RVLM (Figure 4C).

Glutamate and GABA receptor subunit gene expression was compared in active versus sedentary rats (Figures 5-7). Of the five NMDA receptor subunits examined, NR1 ($p = 0.15$) demonstrated a trend towards upregulation with three out of four active animals showing upregulation, and one showing no change (Figure 5A) whereas no significant changes were observed in NR2A ($p = 0.41$), NR2B ($p = 0.56$), NR2C ($p = 0.39$) and NR2D ($p = 0.65$) subunits in active compared to sedentary rats (Figures 5C, 5E, 5G and 5I, respectively). Of the three AMPA receptor subunits examined, GLUR1 ($p = 0.32$), GLUR2 ($p = 0.23$) and GLUR3 ($p = 0.29$) none of them showed significant changes in active compared to sedentary rats (Figures 6C, 6A and 6E respectively). Of the two $GABA_A$ receptor subunits examined,

$GABA_{A1}$ ($p = 0.35$) receptor subunit showed no changes between groups whereas $GABA_{A2}$ ($p = 0.14$) trended towards upregulation with three out of the four animals showing upregulation, and one showing no change in the active rats compared to sedentary rats (Figures 7A and 7C respectively).

The average daily running distance, speed and duration in active rats were 4.49 ± 0.78 km, 39.58 ± 2.07 m/min and 110 ± 19 min, respectively. The average weekly running distance and duration gradually increased until they reached their peak around week 5-8. After 8^{th} week, both the parameters gradually decreased and reached a plateau. The average weekly running speed remained constant throughout the experiment except at the 17^{th} week, where only two animals contributed to the data (Figure 8).

In the group of physically active animals the total running distance ranged from 329 km to 749 km over a 17 week period. Since the amount of voluntary running in active rats may influence the level of gene expression within the RVLM, we performed correlation analyses between total running distance for each rat and corresponding relative gene expression values (i.e. $2^{-\Delta\Delta Ct}$) for glutamate and $GABA_A$ receptor subunits (Figures 5-7). Of the NMDA receptor subunits evaluated, a strong trend towards a positive correlation was observed between the total running distance and NR2C gene expression in the active rats ($R^2 = 0.738$, $p = 0.06$) (Figure 5H). Among the AMPA receptor subunits, GLUR3 showed a significant negative correlation between the total running distance and its relative gene expression in active rats ($R^2 = 0.982$, $p = 0.01$) (Figure 6F). No significant correlation was observed between the total running distance and other NMDA receptor subunits NR1, NR2A, NR2B and NR2D (Figures 5B, 5D, 5F and 5J respectively) or AMPA receptor subunits, GLUR1 and GLUR2 (Figures 6B and 6D respectively). Both $GABA_A$ receptor subunits showed no correlation between the total running distance and gene expression in active rats (Figures 7B and 7D respectively)

3. Discussion

To our knowledge, this is the first study to examine gene expression in spinally-projecting RVLM neurons from sedentary and active rats using LCM. We have determined that bulbospinal RVLM neurons can indeed be identified and obtained using LCM. In addition, isolated RNA from collected cells can be used for gene expression analysis without significant amplification. Interestingly, when AMPA receptors subunits were examined, there was a significant inverse correlation between the amount of voluntary wheel running and gene expression for the GLUR3 subunit of the AMPA receptor.

LCM has been used as a valuable tool in obtaining specific cell types from tissue sections and for studying gene expression profiles (Kerman, Buck, Evans, Akil, and Watson, 2006;Pietersen, Lim, Macey, Woo, and Sonntag, 2011;Yao, Yu, Gong, Taube, Rao, and MacKenzie, 2005). Key studies have laid the foundation for capturing cells using LCM while maintaining the quality and integrity of mRNA, and also avoiding degradation with adequate yield during the LCM process (Kerman, Buck, Evans, Akil, and Watson, 2006;Pietersen, Lim, Macey, Woo, and Sonntag, 2011;Yao, Yu, Gong, Taube, Rao, and MacKenzie, 2005). Thin sections (8 μm) were cryosectioned and only two sections were

placed on each glass slide and dehydrated before the microdissection process. Thin sections aided in ease of identification and collection of cells. Placing only two sections in a slide reduced the amount of time each section was allowed to be at room temperature during capture, hence reducing RNA degradation. The sections were dehydrated to reduce RNAse activity and facilitate removal of the cells from the slide onto the LCM cap. Although staining of sections has been suggested to improve visualization of specific regions or cell types, staining can decreases the integrity of RNA since RNase activity is higher in aqueous environments (Kerman, Buck, Evans, Akil, and Watson, 2006). In the present study, completely separate sets of slides were selected and stained for identifying the location of the RVLM. These sections were not used for capturing cells. The retrograde tracer Fluorogold was injected in the intermediolateral cell column of the spinal cord at the level of T9-T10. This allowed us to visualize spinally projecting cells at the level of the RVLM (Yao, Yu, Gong, Taube, Rao, and MacKenzie, 2005). The captured cells were placed in the lysis buffer and RNA was extracted immediately to diminish degradation. The extracted RNA was converted to cDNA and stored in the -20°C until used for qRT-PCR (see methods).

Using RNA from laser microdissected cells, we were able to detect glutamate and GABA receptor subunit gene expression from both sedentary and active rats. Numerous studies have looked at the changes in the gene expression of these receptor subunits at the level of RVLM under physiological and pathological conditions (Edwards, Loxley, Powers-Martin, Lipski, McKitrick, Arnolda, and Phillips, 2004;Lin, Tsao, and Wang, 1995). However, most of these studies utilized the tissue punch and one of the caveats of using this technique is that the tissue contains a heterogeneous population of neurons and glia making determination of the population in which changes occur difficult. Our approach of using LCM minimizes this problem since we only examined the changes from the cells that are positively identified as spinally-projecting neurons. Furthermore, we only captured cells that were located in a strict rostrocaudal, mediolateral, and dorsoventral region based on well-established criteria from our studies and others in the literature that have identified the location of bulbospinal, barosensitive neurons in the RVLM (refer to Figures 1-3). By doing so, we maximized our chances of capturing populations of somatic profiles that were, at the very least, highly enriched with RNA from neurons involved in sympathetic outflow and blood pressure regulation. In fact, upon post processing of laser captured tissue we observed a number of cell types that were not captured for this study. Since spinal cord injections were restricted to the lower thoracic region (by experimental design), the absence of Fluorogold labeling in a particular cell would not have determined whether the cell was indeed 1) a neuron (versus glia) or 2) whether it projected to other parts of the spinal cord or other parts of the brain. Further phenotyping such as post-processing immunohistochemistry or marker-specific staining, would likely occur at the expense of RNA amount and integrity, something we wanted to avoid in the current study. Nonetheless, these questions are of great interest and we hope to develop methods to additionally characterize laser captured neurons in future studies.

Although there are strong trends in excitatory related genes our findings from the present study do not show differential changes in the gene expression of NMDA, AMPA or GABA receptor subunits in sedentary and active rats. Functional studies from our laboratory showed enhanced sympathoexcitatory responses to glutamate in the sedentary versus physically

active rats (Mischel and Mueller, 2011). Recently, we also found increased dendritic branching in more rostral part of the RVLM in the sedentary compared to active rats (Mischel, Llewellyn-Smith, and Mueller, 2013). The fact that most of the cells collected for gene expression analysis in the present study were from the caudal part of the RVLM may explain the discrepancy since the structural differences in our previous paper were significant at more rostral compared to caudal levels of the ventrolateral medulla (Mischel, Llewellyn-Smith, and Mueller, 2014). Further, it is important to examine changes at both the level of mRNA and protein, especially since alterations in gene expression may not always correlate with changes in protein expression. Also, changes in receptor function can occur via post-translational modifications that could enhance functional responses as observed in a previous study(Dingledine, Borges, Bowie, and Traynelis, 1999) without a change in gene or protein expression.

Finally, correlation data from the present study provided valuable information regarding running distance and changes in the gene expression of certain receptor subunits. In our model, the gene expression data derived from the active group could be variable since the animals do engage in varying levels of voluntary wheel running. This variability in the running distance could be one of the reasons why we did not observe significant differences in gene expression of sedentary versus active rats. Correlation of total running distance to gene expression values of NMDA receptors showed a strong trend ($p=0.06$) for NR2C receptor gene expression. NMDA receptors are tetramers composed of two NR1 and two NR2 subunits. The function of NMDA channels are altered depending on subunit composition(Dingledine, Borges, Bowie, and Traynelis, 1999). Our correlation studies suggested that physical activity positively influences NR2C neuroplasticity in the RVLM, however the mechanisms by which activity mediates the channel properties is unknown. A recent study demonstrated that NMDA channels comprising NR1/NR2C have modest desensitization and low open probability (Dravid, Prakash, and Traynelis, 2008). This finding suggests that increased NR2C might lead to decreased glutamatergic neurotransmission in the RVLM under active conditions. In contrast to NR2C receptor expression, we observed an inverse correlation between running distance and the gene expression levels of the AMPA receptor subunit, GLUR3 in spinally projecting neurons of the RVLM. Though the exact role of GLUR3 in the RVLM-mediated neurotransmission is not clear, knock out studies in mice have suggested that GLUR3 is necessary for maintaining basal synaptic transmission in other brain regions such as the hippocampus (Meng, Zhang, and Jia, 2003). In the absence of GLUR3, there is reduced number of AMPA receptors at the synapse leading to reduced synaptic transmission (Meng, Zhang, and Jia, 2003). This suggests that physical activity may mediate a downregulation of GLUR3's in the RVLM and could reduce basal sympathetic or excitability of RVLM neurons under sympathoexcitatory conditions. We have demonstrated previously both structural (decreased dendritic branching) and functional changes (reduced glutamate responsiveness) in neurons of the RVLM (Mischel, Llewellyn-Smith, and Mueller, 2014;Mischel and Mueller, 2011) may explain some of the cardiovascular benefits of regular exercise and conversely the increased incidence of cardiovascular disease in the sedentary population.

In summary, LCM is an excellent technique that can be used to investigate the gene expression of a specific neuronal population within a heterogeneous tissue, such as the

RVLM. In the present study, we demonstrated the use of LCM to capture spinally-projecting RVLM neurons and studied the changes in gene expression of glutamate and GABA receptors subunits under sedentary and active conditions using qRT-PCR. Further our correlation analysis demonstrates that running distance could indeed affect the gene expression of spinally-projecting RVLM neurons. Overall, these findings suggest that physical activity contributes to neuroplastic changes at the level of RVLM.

4. Experimental Procedure

4.1. Animal Model

Male Sprague-Dawley rats were ordered from Harlan (Indianapolis, IN) at approximately four weeks of age (75-99g). Upon arrival, five animals were randomly designated physically active and singly housed with a commercially available running wheel (Techniplast, Eaton, PA). The animals had 24 hour access to the wheels and therefore ran voluntarily. Running wheel activity was monitored daily by a bike computer (SigmaSport, Olney, IL). Four animals were designated sedentary and were housed similarly but without a running wheel. Both groups of animals were provided food and water ad libitum. The animals were cared for in accordance with the Wayne State University Institutional Animal Care and Use Committee and NIH guidelines.

4.2. Surgical Procedure

After 15-16 weeks of wheel running or sedentary conditions, the animals were prepared for survival surgery. Ketoprofen (Ketofen™, Fort Dodge Animal Health, Fort Dodge, IA; 5mg/kg S.C.) was injected prophylactically in the left hind quarter to reduce pain following surgery. The animal was induced with isoflurane anesthesia (5% with a flow rate of 1.5 liters/min, later reduced to 2% for maintenance) and then injected with atropine (0.05 mg/ml, S.C.) to reduce bronchial secretions. After the surgical site was shaved and cleaned, the skin was cleansed with Povidone iodine and sterile saline, and a sterile drape was placed with only the surgical area exposed. Next, a two-inch incision was made down the midline of the back in the thoracic region. Blunt dissection was used to expose the spinal processes of the thoracic cord. The spinous process of T9 was removed, exposing the T10 spinal cord segment beneath for microinjection. The spinal cord was injected with a retrograde tracer (5 % Fluorogold in saline) targeting the IML (0.8-1 mm lateral to the midline; 1mm below the dorsal surface of the spinal cord). Three injections per side (30 nl each) were spaced rostrocaudally approximately 1 mm apart on each side of the spinal cord (Figure 1). Injections were performed slowly over a period of 1 min and the pipette was left in place for a minimum of five minutes after each injection. After the injection procedure was complete the muscle was sutured with 3-0 monofilament nylon sutures with individual stitches and the skin was closed with wound clips. The animals were placed into their respective cages, given 10 ml of lactated Ringers (s.c.), and half of the cage was placed on a heating pad. Animals were provided loose food pellets and recovery gel (DietGel76A, ClearH20, Portland, MA). Animals were monitored post-surgery and once they were able to maintain sternal recumbency they were returned to the animal facility. The wheel runners were allowed to exercise voluntarily during the recovery period. The sedentary animals remained in their cages without wheel access. The animals were monitored every day following surgery for

normal food and water intake, grooming, and weight gain. Post-operatively, ketoprofen was administered as an analgesic as needed.

4.3. Tissue Removal and Preparation

The animals were monitored for one week post-surgery before they were sacrificed. Fatal plus (50 mg/kg body weight, i.p.) was injected to deeply anesthetize the animal before sacrifice. All the instruments that were used to remove the tissues and blocking the brain were cleaned using RNase-Zap (Life Technologies, Carlsbad, CA) to diminish RNases. Following decapitation, the brain was quickly removed, blocked into segments (i.e., forebrain, midbrain, and brainstem) using a chilled brain matrix (Braintree Scientific, Braintree, MA), and immediately placed in dry ice until frozen. The frozen tissue was stored in a minus 80°C freezer until sectioning.

4.4. Sectioning and Staining

Unsubbed glass slides were numbered, dated, labeled with specific animal information and cleaned with RNase-Zap. The cryostat and the blade used for sectioning were wiped with RNase-Zap before sectioning. The brainstem was taken from the -80°C freezer, mounted on a chuck with OCT and placed in the cryostat set at a temperature of -20°C. Sections (8 μm) were collected onto room temperature slides beginning at the area postrema and ending at the dorsal cochlear nucleus using a rat atlas for reference (Paxinos and Watson, 2007). Two sections were placed on each slide. After completing the sectioning process, slides were selected at 100 μm intervals for cresyl violet staining to identify the location of the RVLM. Using the caudal pole of the facial nucleus as a landmark, slides were selected for laser capture microdissection (Figure 1). Only slides containing sections which were 500 μm caudal or 150 μm rostral to the caudal pole of the facial nucleus were used based on previous reports suggesting this 650 μm region contains spinally-projecting RVLM neurons (Llewellyn-Smith and Mueller, 2013;Mischel, Llewellyn-Smith, and Mueller, 2014;Schreihofer and Sved, 2011).

4.5. Laser Capture Microdissection (LCM)

Brain sections were dehydrated on the slide by rinsing in 4°C acetone (2 min) followed by 70% ethanol (1 min), 95% ethanol (1 min), 100% ethanol (1 min) and xylene (at least 5 min). Once the dehydration was complete, the slide was removed and the xylene was allowed to drain and the slide to dry. In order to optimize RNA recovery, the time that the slide was removed from the xylene to the completion of the LCM procedure was no more than 25-30 minutes. LCM was performed on an Arcturus Pixcell IIe laser capture microscope. First, the slide was placed on the microscope stage and the vacuum was turned on to hold the slide in place. The image was brought into focus using the 10× objective and the coarse and fine microscope adjustment s. The CapSure HS LCM caps (Life Technologies) with the alignment tray was placed into the load line position. After loading the cap, the capping arm was rotated and positioned around the cap.

The region of the RVLM is bounded ventrally by the ventral surface of the medulla, medially by the pyramidal tract, laterally by the spinal trigeminal tract and dorsally by the nucleus ambiguous (Mischel, Llewellyn-Smith, and Mueller, 2014). The slide was adjusted

so that the boundaries of the RVLM were within the capture region (black circle) of the cap. The laser spot size was set to 15 μm and target to 265 mV. The power and duration were set between 45-55 mW and 4.5-5.5 msec respectively for optimal cell capture based on pilot studies from our laboratory.

After enabling the laser, the target spot was visible as a red dot on the computer monitor. The red laser dot was positioned over an area of the slide that does not contain the tissue section and the laser was test-fired until it made a well-defined circle with a clear center. After test-firing the laser, the red laser dot was scrolled over the RVLM region to capture Fluorogold-positive neurons. A filter cube for wide UV excitation and long-pass emission was used to view Fluorogold-positive neurons (Yao, Yu, Gong, Taube, Rao, and MacKenzie, 2005). Spinally projecting RVLM neurons were defined as cells containing a clear nucleus surrounded by punctate fluorescence in the cytoplasm. After capturing the cells within the black circle, the capping arm was lifted, separating the captured cells from the section and adhering them to the cap membrane (Figure 3). The cap membrane was peeled away from the cap and placed in RNase-free microcentrifuge tube filled with 100 μl lysis solution in ice.

4.6. RNA Isolation and Quantification

After collecting the cells, the sample was incubated for 30 min at 42°C to disrupt cell membranes and allow access to the RNA contained within the cell for stabilization. RNA from cells was isolated using RNAqueous-Micro Kit (Life Technologies, Carlsbad, CA) following the manufacturer's protocol. The micro filter cartridge assembly was pre-wet with 30 μl of lysis solution directed towards the center of the filter. After 5 minutes, the tube was centrifuged for 30 seconds at 10,000 × g. LCM additive (3 μl) was added to the lysate and mixed well. The mixture was briefly centrifuged to collect the fluid at the bottom of the tube. 100% ethanol (52 μl) was added to the sample lysate mixture and gently vortexed. The entire mixture was loaded onto the prepared cartridge assembly and the cap was closed. The filter column was centrifuged for 1 min at 10,000 × g for 1 min to bind the RNA to the filter. After the wash steps, the residual fluid was removed and the filter was dried according to manufacturer's protocol. The elution solution was preheated to 95°C and added (10 μl) to the center of the filter. The filter was placed at room temperature for 5 min. The assembly was centrifuged for 1 min to elute the RNA from the filter. The last step was repeated with another 10 μl of preheated elution solution and collected in the same micro elution tube. In addition to the manufacturer's recommendation the last step was repeated using another 10 μl of preheated elution solution and stored in a separate tube. RNA was quantified using a Nanodrop ND-1000 spectrophotometer (Thermo Scientific, Wilmington, DE). The purity of the RNA sample was assessed using 260/280 ratio. Samples with a 260/280 ratio within the range of 1.5 to 2.5 were used for further processing.

4.7. RNA to cDNA Conversion and quantitative real-time PCR (qRT-PCR)

Total RNA (250 ng) was converted into cDNA using high capacity cDNA reverse transcription kit (Life Technologies, Carlsbad, CA) following the manufacturer's protocols. Equal volumes of total RNA (50 μl) and RT master mix (50 μl) was added for a total reaction volume of 100 μl and reverse transcription was performed using a thermal cycler

(Eppendorf) under the following conditions: 25°C (10 min) and 37°C (120 min). The cDNA obtained from the above process was stored at -20°C until used for qRT-PCR. For long-term storage, the samples were stored at -80°C.

For the genes of interest, qRT-PCR was performed using a Mastercycler EP Realplex machine (Eppendorf). The TaqMan primer/probe assays for glutamate receptors subtypes including NMDA receptor genes (NR1, NR2A-D), AMPA receptors genes (GLUR1, GLUR2, GLUR3), and GABA receptors genes including $GABA_{A\alpha1}$ ($GABA_{A1}$), $GABA_{A\alpha2}$ ($GABA_{A2}$) and the housekeeping gene HPRT (hypoxanthine guanine phosphoribosyl transferase) were used (Taqman Assays-on-Demand, Applied Biosystems, Foster City, CA). Each gene was probed separately. The PCR reaction mix contained 3 μl of cDNA, 8.25 μl of DEPC water, 12.5 μl of Taqman Universal PCR Master Mix™ (Applied Biosystems, Foster City, CA) and 1.25 μl of specific Taqman™ assay probe for a total reaction volume of 25 μl. Each sample was run in triplicate. The PCR plates with 96 wells were run on the PCR machine with the following program: 50°C (2 min), 95°C (10 min) one cycle, 92°C (15 sec), 60°C (1 min) 40 cycles. The relative changes in gene expression between the sedentary and active groups were analyzed using $2^{-\Delta\Delta Ct}$ method (Livak and Schmittgen, 2001). A student's t-test was performed to evaluate the changes between the groups. A p value < 0.05 was considered statistically significant.

In both sedentary and active groups the delta Ct values for the genes of interest was obtained by subtracting the average Ct values to its respective house- keeping gene HPRT. The delta delta Ct values in the sedentary animals were obtained by subtracting the average delta Ct value from the control group (i.e. sedentary) (Livak and Schmittgen, 2001). This resulted in all the delta delta Ct values for the genes of interest in the sedentary animal to be zero and its $2^{-\Delta\Delta Ct}$ values normalized to 1. The delta delta Ct values in the active animals were also obtained by subtracting the average delta Ct value from the sedentary group. The $2^{-\Delta\Delta Ct}$ values were obtained individually for the genes of interest in the active group and their mean value was shown in figures 5-7 along with sedentary group as control.

Acknowledgments

The authors would like to thank Dr. Robert Mackenzie for kindly allowing us to use the Arcturus Pixcell IIe laser capture microscope. We would also like to acknowledge the help of the following individuals from the Mueller laboratory for excellent technical assistance: Toni Azar, Erin Skotzke and Nathan Vengalil. This work was supported by grant from the National Heart, Lung and Blood Institute, National Institutes of Health, Award Number R01HL096787, to PJM and NIDCD, NIH Award Number DC0077331, to AGH.

References

Zucker IH, Wang W, Brandle M, Schultz HD, Patel KP. Neural regulation of sympathetic nerve activity in heart failure. Prog Cardiovasc Diseases. 1995; 37:397–414.

Fisher JP, Young CN, Fadel PJ. Central sympathetic overactivity: maladies and mechanisms. Auton Neurosci. 2009; 148:5–15. [PubMed: 19268634]

Malpas SC. Sympathetic nervous system overactivity and its role in the development of cardiovascular disease. Physiol Rev. 2010; 90:513–557. [PubMed: 20393193]

Martins-Pinge MC, Becker LK, Garcia MR, Zoccal DB, Neto RV, Basso LS, de Souza HC, Lopes OU. Attenuated pressor responses to amino acids in the rostral ventrolateral medulla after swimming training in conscious rats. Auton Neurosci. 2005; 122:21–28. [PubMed: 16139573]

Mueller PJ. Physical (in)activity-dependent alterations at the rostral ventrolateral medulla: influence on sympathetic nervous system regulation. Am J Physiol Regul Integr Comp Physiol. 2010; 298:R1468–R1474. [PubMed: 20357021]

Guyenet PG. The sympathetic control of blood pressure. Nat Rev Neurosci. 2006; 7:335–346. [PubMed: 16760914]

Dampney RA. Blood pressure regulation by C1 neurons in the rostral ventrolateral medulla: new light on the subject. J Physiol. 2009; 587:5513. [PubMed: 19959547]

Amendt K, Czachurski J, Dembowsky K, Seller H. Bulbospinal projections to the intermediolateral cell column: a neuroanatomical study. J Auton Nerv Syst. 1979; 1:103–107. [PubMed: 575994]

Lipski J, Kanjhan R, Kruszewska B, Smith M. Barosensitive neurons in the rostral ventrolateral medulla of the in vivo: morphological properties and relationship to C1 adrenergic neurons. Neuroscience. 1995; 69:601–618. [PubMed: 8552253]

Dampney RAL. Functional organization of central pathways regulating the cardiovascular system. Physiol Rev. 1994; 74:323–364. [PubMed: 8171117]

Guyenet, PG., Stornetta, RL. The presympathetic cells of the rostral ventrolateral medulla (RVLM): anatomy, physiology and role in the control of circulation. In: Dun, NJ.Machado, BH., Pilowsky, PM., editors. Neural Mechanisms of Cardiovascular Regulation. Kluwer Academic Publishers; Norwell, MA: 2004. p. 187-218.

Pilowsky PM, Abbott SB, Burke PG, Farnham MM, Hildreth CM, Kumar NN, Li Q, Lonergan T, McMullan S, Spirovski D, Goodchild AK. Metabotropic neurotransmission and integration of sympathetic nerve activity by the rostral ventrolateral medulla in the rat. Clin Exp Pharmacol Physiol. 2008; 35:508–511. [PubMed: 18307751]

Sved AF. Tonic glutamatergic drive of RVLM vasomotor neurons? Am J Physiol Regul Integr Comp Physiol. 2004; 287:R1301–R1303. [PubMed: 15528400]

Stornetta RL, Sevigny CP, Schreihofer AM, Rosin DL, Guyenet PG. Vesicular glutamate transporter DNPI/VGLUT2 is expressed by both C1 adrenergic and nonaminergic presympathetic vasomotor neurons of the rat medulla. J Comp Neurol. 2002; 444:207–220. [PubMed: 11840475]

Edwards MA, Loxley RA, Powers-Martin K, Lipski J, McKitrick DJ, Arnolda LF, Phillips JK. Unique levels of expression of N- methyl-D-aspartate receptor subunits and neuronal nitric oxide synthase in the rostral ventrolateral medulla of the spontaneously hypertensive rat. Brain Res Mol Brain Res. 2004; 129:33–43. [PubMed: 15469880]

Hermes SM, Mitchell JL, Silverman MB, Lynch PJ, McKee BL, Bailey TW, Andresen MC, Aicher SA. Sustained hypertension increases the density of AMPA receptor subunit, GluR1, in baroreceptive regions of the nucleus tractus solitarii of the rat. Brain Res. 2008; 1187:125–136. [PubMed: 18031714]

Kiely JM, Gordon FJ. Non-NMDA receptors in the rostral ventrolateral medulla mediate somatosympathetic pressor responses. J Auton Nerv Syst. 1993; 43:231–240. [PubMed: 7690055]

Miyawaki T, Minson J, Arnolda L, Llewellyn-Smith I, Chalmers J, Pilowsky P. AMPA/kainate receptors mediate sympathetic chemoreceptor reflex in the rostral ventrolateral medulla. Brain Res. 1996; 726:64–68. [PubMed: 8836546]

Wang WZ, Wang LG, Gao L, Wang W. Contribution of AMPA/kainate receptors in the rostral ventrolateral medulla to the hypotensive and sympathoinhibitory effects of clonidine. Am J Physiol Regul Integr Comp Physiol. 2007; 293:R1232–R1238. [PubMed: 17581836]

Farmer J, Zhao X, Van Praag H, Wodtke K, Gage FH, Christie BR. Effects of voluntary exercise on synaptic plasticity and gene expression in the dentate gyrus of adult male Sprague-Dawley rats *in vivo*. Neuroscience. 2004; 124:71–79. [PubMed: 14960340]

Li YF, Cornish KG, Patel KP. Alteration of NMDA NR_1 receptors within the paraventricular nucleus of hypothalamus in rats with heart failure. Cir Res. 2003; 93:990–997.

Kleiber AC, Zheng H, Schultz HD, Peuler JD, Patel KP. Exercise training normalizes enhanced glutamate-mediated sympathetic activation from the PVN in heart failure. Am J Physiol Regul Integr Comp Physiol. 2008; 294:R1863–R1872. [PubMed: 18385465]

Malinow R, Malenka RC. AMPA receptor trafficking and synaptic plasticity. Annu Rev Neurosci. 2002; 25:103–126. [PubMed: 12052905]

Wang WZ, Gao L, Wang HJ, Zucker IH, Wang W. Tonic glutamatergic input in the rostral ventrolateral medulla is increased in rats with chronic heart failure. Hypertension. 2009; 53:370–374. [PubMed: 19029485]

Mischel NA, Mueller PJ. (In)activity-dependent alterations in resting and reflex control of splanchnic sympathetic nerve activity. J Appl Physiol. 2011; 111:1854–1862. [PubMed: 21979802]

Mueller PJ, Mischel NA. Selective enhancement of glutamate-mediated pressor responses after GABA(A) receptor blockade in the RVLM of sedentary versus spontaneous wheel running rats. Front Physiol. 2012; 3:447. [PubMed: 23189062]

Miyawaki T, Goodchild AK, Pilowsky PM. Evidence for a tonic GABA-ergic inhibition of excitatory respiratory-related afferents to presympathetic neurons in the rostral ventrolateral medulla. Brain Res. 2002; 924:56–62. [PubMed: 11743995]

Dampney RAL, Blessing WW, Tan E. Origin of tonic GABAergic inputs to vasopressor neurons in the subretrofacial nucleus of the rabbit. J Auton Nerv Syst. 1988; 24:227–239. [PubMed: 3209808]

Foley CM, Stanton JJ, Price EM, Cunningham JT, Hasser EM, Heesch CM. GABA(A) alpha1 and alpha2 receptor subunit expression in rostral ventrolateral medulla in nonpregnant and pregnant rats. Brain Res. 2003; 975:196–206. [PubMed: 12763608]

Li DP, Pan HL. Plasticity of GABAergic control of hypothalamic presympathetic neurons in hypertension. Am J Physiol Heart Circ Physiol. 2005; 290:H1110–H1119. [PubMed: 16243912]

Nakamura T, Kawabe K, Sapru HN. Cold pressor test in the rat: medullary and spinal pathways and neurotransmitters. Am J Physiol Heart Circ Physiol. 2008; 295:H1780–H1787. [PubMed: 18757476]

Moffitt JA, Heesch CM, Hasser EM. Increased $GABA_A$ inhibition of the RVLM following hindlimb unloading in rats, Am. J Physiol. 2002; 283:R604–R614.

Mueller PJ. Exercise training and sympathetic nervous system activity: evidence for physical activity dependent neural plasticity. Clin Exp Pharmacol Physiol. 2007; 34:377–384. [PubMed: 17324153]

Smith JK, Barron KW. Cardiovascular effects of L-glutamate and tetrodotoxin microinjected into the rostral and caudal ventrolateral medulla in normotensive and spontaneously hypertensive rats. Brain Res. 1990; 506(1):1–8. [PubMed: 1967961]

Huber DA, Schreihofer AM. Altered regulation of the rostral ventrolateral medulla in hypertensive obese Zucker rats. Am J Physiol Heart Circ Physiol. 2011; 301:H230–H240. [PubMed: 21536848]

Schreihofer, AM., Sved, AF. The ventrolateral medulla and sympathetic regulation of arterial pressure. In: Llewellyn-Smith, IJ., Verberne, AJM., editors. Autonomic control of cardiovascular function. Oxford University Press; New York: 2011. p. 78-97.

Emmert-Buck MR, Bonner RF, Smith PD, Chuaqui RF, Zhuang Z, Goldstein SR, Weiss RA, Liotta LA. Laser capture microdissection. Science. 1996; 274:998–1001. [PubMed: 8875945]

Llewellyn-Smith IJ, Mueller PJ. Immunoreactivity for the NMDA NR1 subunit in bulbospinal catecholamine and serotonin neurons of rat ventral medulla. Auton Neurosci. 2013

Kerman IA, Buck BJ, Evans SJ, Akil H, Watson SJ. Combining laser capture microdissection with quantitative real-time PCR: effects of tissue manipulation on RNA quality and gene expression. J Neurosci Methods. 2006; 153:71–85. [PubMed: 16337273]

Yao F, Yu F, Gong L, Taube D, Rao DD, MacKenzie RG. Microarray analysis of fluoro-gold labeled rat dopamine neurons harvested by laser capture microdissection. J Neurosci Methods. 2005; 143:95–106. [PubMed: 15814141]

Pietersen CY, Lim MP, Macey L, Woo TU, Sonntag KC. Neuronal type-specific gene expression profiling and laser-capture microdissection. Methods Mol Biol. 2011; 755:327–343. [PubMed: 21761317]

Lin JC, Tsao WL, Wang Y. Cardiovascular effects of NMDA in the RVLM of spontaneously hypertensive rats. Brain Res Bull. 1995; 37:289–294. [PubMed: 7627572]

Mischel NA, Llewellyn-Smith IJ, Mueller PJ. Physical (in)activity dependent structural plasticity in bulbospinal catecholaminergic neurons of rat rostral ventrolateral medulla. J Comp Neurol. 2013 in press.

Mischel NA, Llewellyn-Smith IJ, Mueller PJ. Physical (in)activity-dependent structural plasticity in bulbospinal catecholaminergic neurons of rat rostral ventrolateral medulla. J Comp Neurol. 2014; 522:Spc1. [PubMed: 24723248]

Dingledine R, Borges K, Bowie D, Traynelis SF. The glutamate receptor ion channels. Pharmacol Rev. 1999; 51:7–61. [PubMed: 10049997]

Dravid SM, Prakash A, Traynelis SF. Activation of recombinant NR1/NR2C NMDA receptors. J Physiol. 2008; 586:4425–4439. [PubMed: 18635641]

Meng Y, Zhang Y, Jia Z. Synaptic transmission and plasticity in the absence of AMPA glutamate receptor GluR2 and GluR3. Neuron. 2003; 39:163–176. [PubMed: 12848940]

Paxinos, G., Watson, C. The rat brain in stereotaxic coordinates. Elsevier Inc; Burlington, MA: 2007.

Livak KJ, Schmittgen TD. Analysis of relative gene expression data using real-time quantitative PCR and the 2(-Delta Delta C(T)) Method. Methods. 2001; 25:402–408. [PubMed: 11846609]

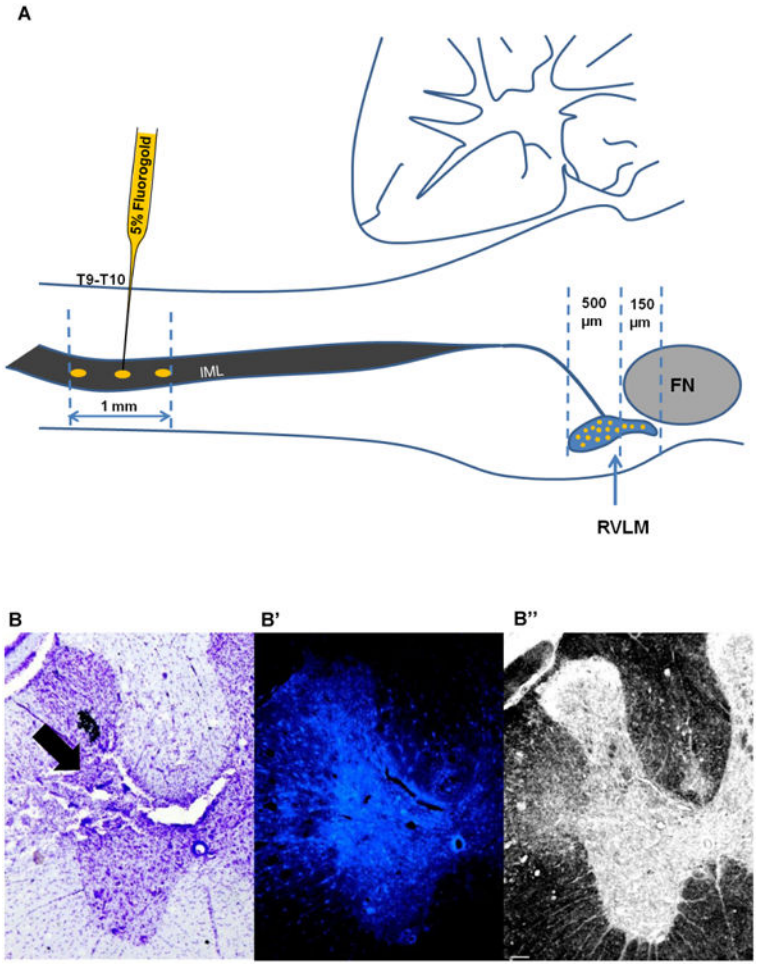

Figure 1. Fluorogold injections at T9-T10 of the spinal cord

A) Schematic representation of Fluorogold injection (1mm from the dorsal surface - gold ovals) into the intermediolateral cell column (IML) of the spinal cord. Fluorogold (5%) was injected using a glass micropipette at the level of T9-T10, where neurons from the RVLM (gold filled circles) send their projections. Fluorogold labeled neurons were found throughout the rostro-caudal extent of the RVLM. Fewer cells were captured from 150µm rostral to caudal pole of Facial Nucleus (FN) compared to the region of the RVLM that lie 500µm caudal to the caudal pole of the FN. Diagram modified from Dampney, 1994. B) Representative Cresyl violet stained section of the spinal cord showing the injection site (black arrow) at the level of T9. B′) Fluorescent section adjacent to section in Figure B, showing the fluorescence intensity in the injection site (white arrow) at the level of T9. B") Bright field image of the same section shown in B′ demonstrating the changes in tissue architecture at the level of injection site (black arrow). Scale bar, 100 µm. cc=central canal; DH=dorsal horn; IML=intermediolateral cell column; VH=ventral horn.

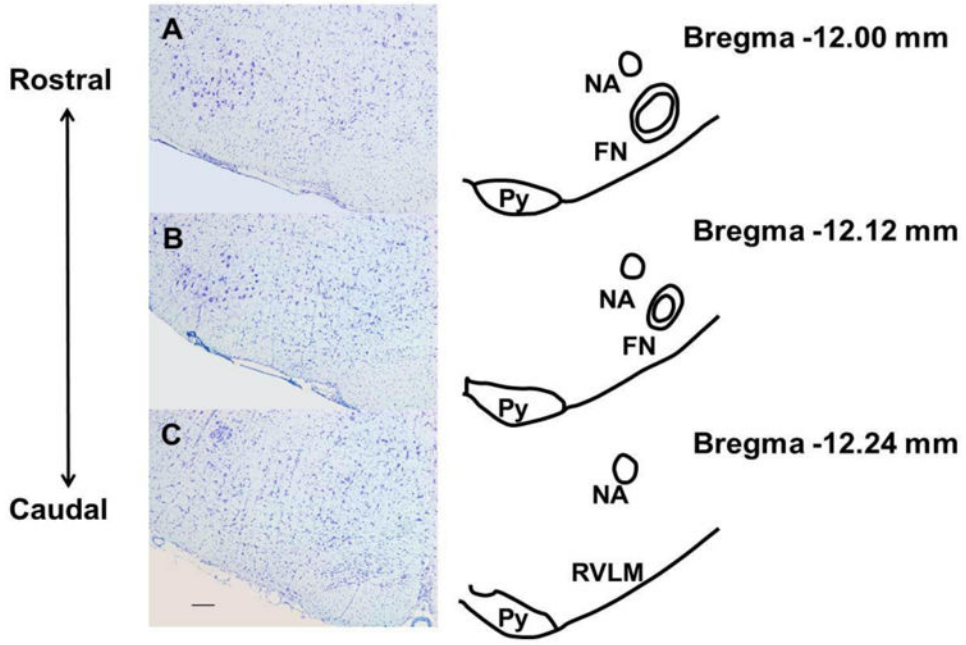

Figure 2. Histological localization of the caudal pole of facial nucleus

Cresyl violet stained sections separated by 120 μm were paired with corresponding schematics from a rat atlas (Paxinos and Watson, 2007). These sections represent regions rostral (Sections A and B) and caudal (Section C) to the caudal pole of the facial nucleus and were used to identify the sections for laser capture microdissection, which encompassed the rostro-caudal extent of the RVLM. (FN, Facial nucleus; Py, pyramidal tract; NA, nucleus ambiguus). Scale bar, 200 μm.

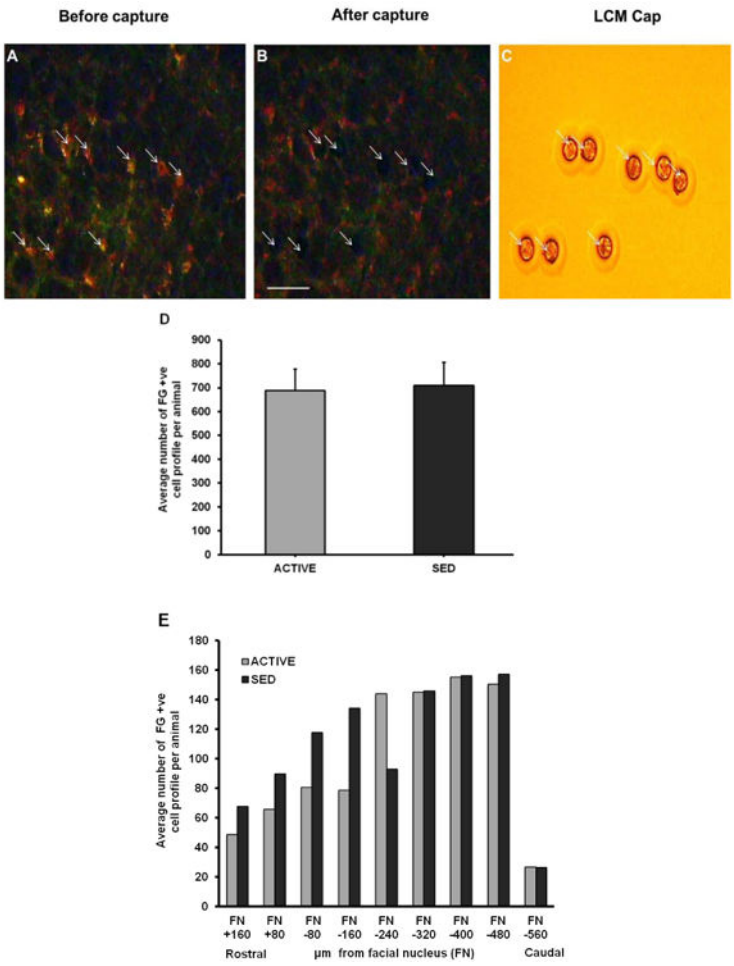

Figure 3. Laser capture microdissection in brainstem sections containing RVLM

A) Representative section of Fluorogold-positive (FG +ve) neurons (arrows) before laser capture microdissection. B) Brainstem section following laser capture showing areas of removed cells (arrows). C) Captured cells are shown on the LCM cap (arrows). Scale bar, 100 μm. D) Representative section of post capture tissue demonstrating areas of cell capture within the predefined boundaries of the RVLM as described in the Methods section. Inset (D′) shows eight somatic profiles captured by the laser (D”=2× enlarged version of D′). E) Same tissue section from Figure 3D that was stained with Cresyl violet. Inset (E′) demonstrates capture of specific cell types (i.e. Fluorogold positive) and not other cell types located within and outside the region of the RVLM (compare identical location of capture sites numbered 1-8 in Figures 3D′ and 3E′) (E”=2× enlarged version of E′). Scale bar= 200 μm; NA=nucleus ambiguus; RVLM=rostral ventrolateral medulla; Py=Pyramidal tract.

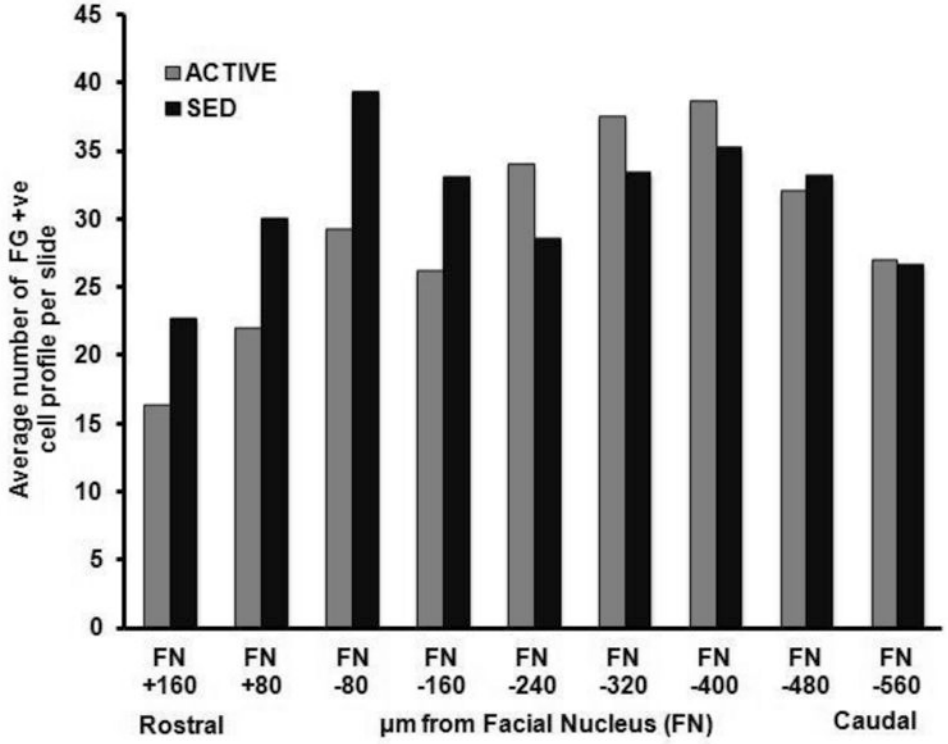

Figure 4. Rostrocaudal distribution of spinally projecting cells collected via LCM in the RVLM

A) Bar graphs representing the average number of cells that were collected between sedentary and active rats. Data presented as mean ± S.E. B) Bar graphs represent the average number of cells collected in active and sedentary rats in a rostro-caudal manner. For ACTIVE:SED respectively n= 1:1 (FN +160), 1:1 (FN +80), 2:1 (FN -80), 4:2 (FN -160), 5:4 (FN -240), 5:4 (FN -320), 5:4 (FN -400), 4:4 (FN -480), 1:3 (FN -560). The number of animals precluded formal statistical analysis. C) Bar graphs represent the average number of Fluorogold-positive (FG +ve) cells collected per slide at each rostrocaudal level taken from active and sedentary animals. For ACTIVE:SED respectively n= 1:1 (FN +160), 1:1 (FN +80), 2:1 (FN -80), 4:2 (FN -160), 5:4 (FN -240), 5:4 (FN -320), 5:4 (FN -400), 4:4 (FN -480), 1:3 (FN -560). The number of animals precluded formal statistical analysis.

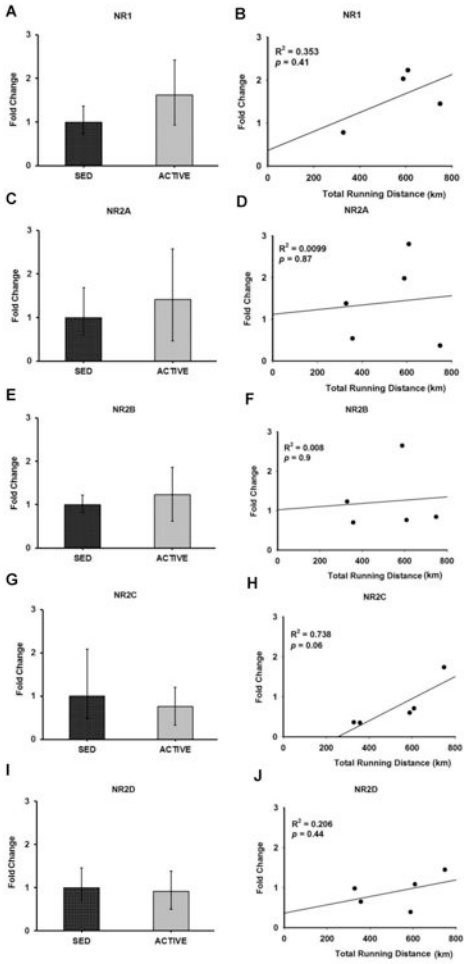

Figure 5. Gene expression and correlation of NMDA receptor subunits in the RVLM

Bar graphs compare the gene expression of NMDA receptor subunits NR1 (A), NR2A (C), NR2B (E), NR2C (G) and NR2D (I) in spinally-projecting RVLM neurons between sedentary and active rats measured by real-time qRT-PCR. Data presented as fold change ± S.D. Correlation was determined between the total running distance in active animals and fold change of NMDA receptor subunits NR1 (B), NR2A (D), NR2B (F), NR2C (H), and NR2D (J) in spinally-projecting RVLM neurons. Gene expression of NR2C showed a positive correlation trend towards the total running distance ($p = 0.06$) suggesting that physical activity could contribute to NR2C neuroplasticity in the RVLM.

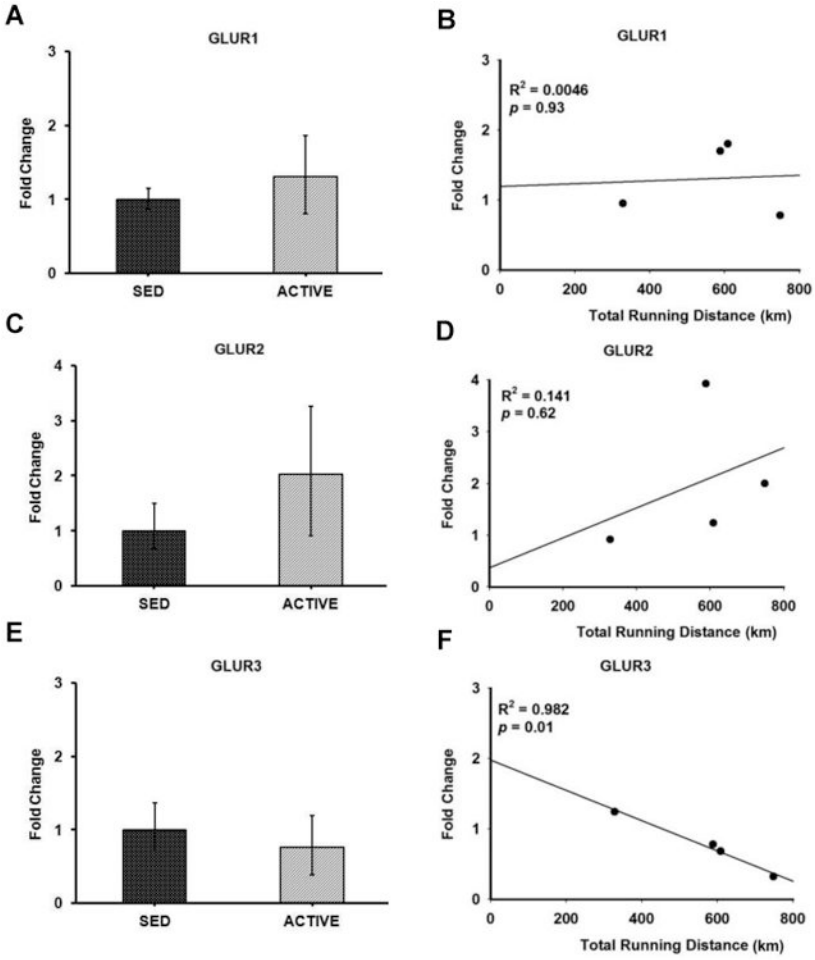

Figure 6. Gene expression and correlation of AMPA receptor subunits in the RVLM

Bar graphs compare the gene expression of AMPA receptor subunits GLUR1 (A), GLUR2 (C) and GLUR3 (E) in spinally-projecting RVLM neurons between sedentary and active rats measured by real-time qRT-PCR. Data presented as fold change ± S.D. Correlation was determined between the total running distance in active animals and fold change of AMPA receptor subunits GLUR1 (B), GLUR2 (D) and GLUR3 (F) in spinally-projecting RVLM neurons. Gene expression of GLUR3 showed inverse correlation with the total running distance ($p = 0.01$) suggesting that physical activity could contribute to GLUR3 neuroplasticity in the RVLM.

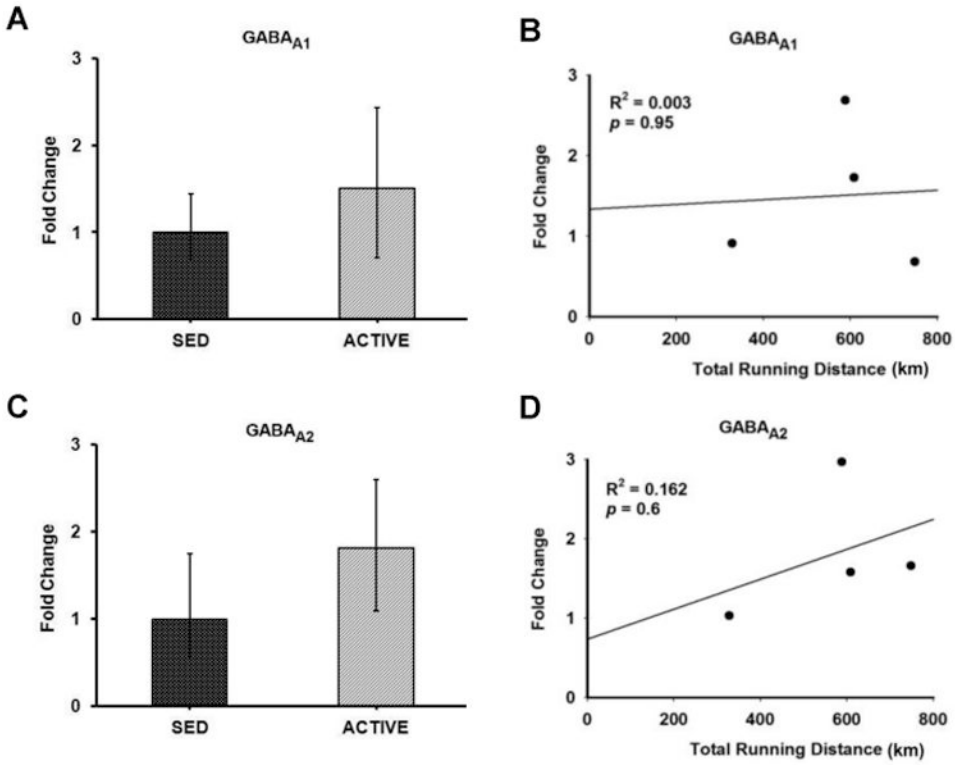

Figure 7. Gene expression and correlation of GABA$_A$ receptor subunits in the RVLM

Bar graphs compare the gene expression of GABA$_A$ receptor subunits GABA$_{A1}$ (A) and GABA$_{A2}$ (C) in spinally-projecting RVLM neurons between sedentary and active rats measured by real-time qRT-PCR. Data presented as fold change ± S.D. Correlation was determined between the total running distance in active animals and fold change of GABA$_A$ receptor subunits GABA$_{A1}$ (B) and GABA$_{A2}$ (D) in spinally-projecting RVLM neurons. No correlation was observed between the running distance and gene expression of GABA$_A$ receptor subunits in the RVLM.

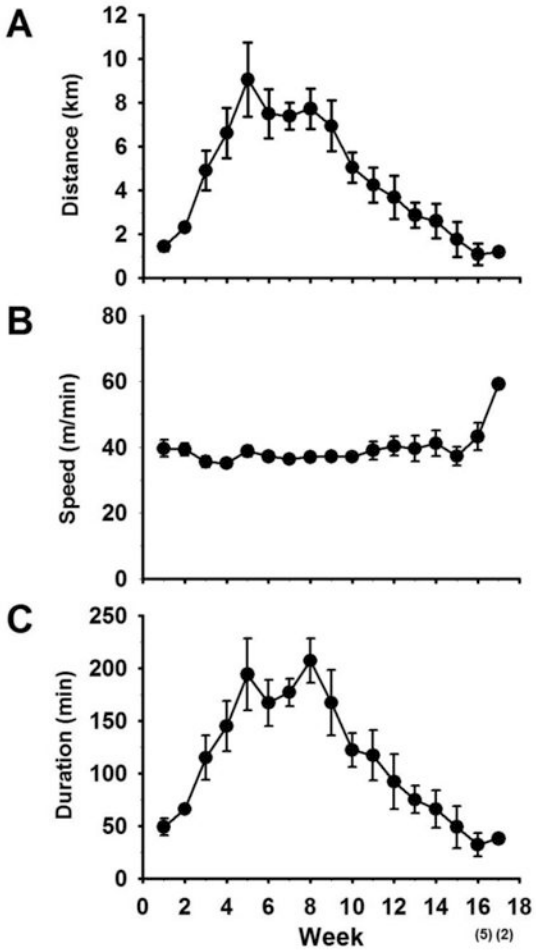

Figure 8. Average running distance over the course of the experiment

The average weekly running distance (A) along with speed (B) and duration (C) are given here. Number of animals that contributed to the data was given within bracket in the x-axis.